Microchemical Journal 204 (2024) 111129

Contents lists available at ScienceDirect

Microchemical Journal

journal homepage: www.elsevier.com/locate/microc

Exploiting the pH-responsive behavior of zinc-dithizone complex for fluorometric urea sensing utilizing red-emission carbon dots

Khalid Alhazzani [a], Ahmed Z. Alanazi [a], Aya M. Mostafa [b,c], James Barker [b], Hossieny Ibrahim [d,e], Mohamed M. El-Wekil [c], Al-Montaser Bellah H. Ali [c,*]

[a] Department of Pharmacology and Toxicology, College of Pharmacy, King Saud University, Riyadh, Saudi Arabia
[b] School of Life Sciences, Pharmacy, and Chemistry, Kingston University, Kingston-upon-Thames, London KT1 2EE, UK
[c] Department of Pharmaceutical Analytical Chemistry, Faculty of Pharmacy, Assiut University, Assiut, Egypt
[d] Department of Chemistry, Faculty of Science, Assiut University, Assiut 71516, Egypt
[e] School of Biotechnology, Badr University in Assiut, Assiut 2014101, Egypt

ARTICLE INFO

Keywords:
Fluorescence
Carbon dots
Zinc-dithizone
Urea
Urease

ABSTRACT

This study develops a novel fluorometric method for the sensitive and selective determination of urea, based on unique system comprising nitrogen doped red-emissive carbon dots (NRECDs), zinc-dithizone complex, and the urease enzyme. The underlying principle of this method relies on the pH increase resulting from the enzymatic breakdown of urea by urease. Initially, the fluorescence of the NRECDs is quenched by the red-colored zinc-dithizone complex. However, upon the addition of urea, the subsequent release of ammonia and the consequent rise in pH lead to the dissociation of the zinc-dithizone complex, causing a color change from red to yellow. This spectral shift eliminates the quenching effect, resulting in the restoration of the CDs' fluorescence. The prepared NRECDs were comprehensively characterized using various spectroscopic techniques, including fluorometry, X-ray diffraction (XRD), X-ray photoelectron spectroscopy (XPS), UV–visible spectroscopy, and transmission electron microscopy (TEM) imaging. The proposed fluorometric method exhibits excellent sensitivity (Limit of detection = 0.0012 mM) and linearity (R^2 = 0.9951) in the determination of urea. Notably, this approach addresses the selectivity limitations of previous pH-sensitive CDs-based methods, which relied solely on the intrinsic response of CDs, lacking specificity in either quenching or fluorescence enhancement. Furthermore, the developed method demonstrates remarkable selectivity, as evidenced by negligible interference from various potentially interfering substances, ensuring reliable and accurate urea quantification. When applied to human serum samples, the method showcased excellent recovery with low relative standard deviations, highlighting its practical applicability in biomedical and clinical applications.

1. Introduction

Urea is a vital organic compound that plays a crucial role in mammalian metabolism. It serves as the primary vehicle for the elimination of waste nitrogen from the body, making it an essential component of the urea cycle [1]. Urea is produced in the liver from ammonia and subsequently excreted through the kidneys, highlighting its significance in maintaining the body's nitrogen balance and overall health. The typical range of urea levels in human blood falls within 2.5 to 7.1 mM [2]. However, deviations from this range can occur in various pathophysiological conditions. Elevated levels of urea, known as uremia or azotemia, are commonly observed in cases of renal dysfunction, dehydration, or increased protein catabolism. In contrast, decreased levels of urea may indicate severe liver disease or malnutrition, as the liver is responsible for synthesizing urea from ammonia. Prolonged exposure to high urea levels can lead to serious complications, such as electrolyte imbalances, fluid retention, metabolic acidosis, and uremic syndrome, which is characterized by fatigue, nausea, and neurological symptoms. Urea levels in urine can also provide valuable diagnostic information. Normally, urea concentration in urine is significantly higher than in blood, typically ranging from 333 to 667 mM in healthy individuals. Elevated urinary urea levels can indicate high protein intake, enhanced protein catabolism, or increased urea production due to certain metabolic conditions. Conversely, low urinary urea levels may

* Corresponding author.
E-mail address: Almontaser_bellah@aun.edu.eg (A.-M.B.H. Ali).

https://doi.org/10.1016/j.microc.2024.111129
Received 11 May 2024; Received in revised form 2 July 2024; Accepted 4 July 2024
Available online 5 July 2024

suggest impaired kidney function, as the kidneys are less able to excrete urea efficiently, or may indicate a low-protein diet or malnutrition [3]. The monitoring of urea levels is of major significance in several applications [3]. In the environmental field, urea is widely used as a nitrogen-rich fertilizer, and its accurate quantification is essential for agricultural and environmental monitoring. Additionally, the quantitation of urea levels in blood and urine is a vital diagnostic tool for assessing renal function, monitoring kidney diseases, and evaluating metabolic disorders in the medical field [4].

Urease, an enzymatic catalyst that promotes the hydrolysis of urea, yielding carbon dioxide and ammonia, is a key component in the measurement of urea levels [5]. By facilitating the conversion of urea into measurable products, urease enables the development of various analytical methods for urea determination [6]. These methods include potentiometric ammonium ion-selective electrodes [7], pH electrodes, ammonia gas electrodes [8], and amperometry [9]. Additional methods such as chromatography [10], electrochemical techniques [11], spectroscopic [12], and fluorometric methods [13,14] were also employed for the determination of urea. While these existing methods have contributed to the analysis of urea, they often face significant limitations. For instance, some techniques suffer from interference from other compounds present in complex matrices, leading to reduced selectivity and accuracy. Others may be hindered by high costs, complex instrumentation, or limited sensitivity.

Quasi-spherical carbon nanoparticles, with dimensions typically under 10 nm, form a class of luminescent nanomaterials known as carbon dots. These tiny particles possess unique optical properties, including bright and tunable fluorescence, excellent photostability, and good biocompatibility. Their low toxicity profile, cost-effective production, and ease of surface modification contribute to the attractiveness of carbon dots in fields such as bioimaging, sensing, catalysis, and optoelectronic devices [15,16]. Carbon dots can be synthesized through a number of methods, which includes top-down approaches like arc discharge and laser ablation, or bottom-up techniques like hydrothermal carbonization, microwave-assisted pyrolysis, and combustion methods [17,18].

Previous methods for urea detection based on carbon dots primarily relied on the quenching of carbon dot fluorescence upon the release of ammonia in the presence of urease [19–23]. While this approach has been widely explored, it suffers from several limitations. The quenching mechanism often lacks specificity, as various quenchers can potentially influence the fluorescence intensity, leading to inaccurate results. Additionally, the presence of autofluorescence species in biological matrices can interfere with either excitation or emission spectra, affecting the reliability of the obtained fluorescence emission intensities. Furthermore, the complexity of preparation for some probes poses another challenge. In contrast, the proposed method introduces a novel approach that overcomes these limitations by utilizing nitrogen doped red emission carbon dots (NRECDs) that are stable over a wide pH range, particularly in alkaline conditions. This stability allows for the implementation of a colorimetric detection strategy utilizing the pH-induced color change of the zinc-dithizone complex. In addition, the utilization of red-emissive carbon dots, with an excitation wavelength of 565 nm and an emission wavelength of 612 nm, circumvents the issue of autofluorescence species interfering with either the excitation or emission spectra. Upon the liberation of ammonia from the urease-mediated hydrolysis of urea, the pH of the solution increases, causing the zinc-dithizone complex to undergo a noticeable color change from red to yellow. The proposed method ingeniously combines the unique properties of NRECDs with the pH-induced color change of the zinc dithizone complex. Initially, the red colored zinc dithizone complex acts as an efficient quencher, suppressing the fluorescence of the NRECDs. However, upon the liberation of ammonia from the urease-mediated hydrolysis of urea, the pH of the solution increases, causing the zinc dithizone complex to undergo a distinct color change from red to yellow. This color transition disrupts the quenching interaction, leading to the restoration of the carbon dots' fluorescence signal. Consequently, the fluorescence intensity of the NRECDs is recovered, providing a quantifiable optical response directly correlated with the concentration of urea in the human serum and urine samples.

2. Experimental

2.1. Materials and reagents

Urease (EC 3.5.1.5) from Canavalia ensiformis (Jack bean) was obtained from Sigma-Aldrich Chemical Co. (Steinheim, Germany). The enzyme had a specific activity of 50,000 units/g solid, where one unit of urease is defined as the amount of enzyme that liberates 1 μmol of NH_3 from urea per minute at pH 7.0 and 25 °C. O-phenylene diamine (OPD), semicarbazide, acetone, urea, sodium dodecyl sulfate (SDS), zinc sulphate and dithizone were procured from El-Naser Co. Cario, Egypt. Sodium dihydrogen phosphate (NaH_2PO_4), disodium hydrogen phosphate (N_2HPO_4), alanine, glycine, threonine, arginine, histidine, lysine, phenylalanine, fructose, glucose, and human serum protein were supplied from Alpha Chemia (Mumbai, India). The double distilled water (DDW) used in all procedures offered a resistivity around 18 MΩ cm.

2.2. Instrumentation

Details of the instrumentation used in the study are provided in the supplementary data file.

2.3. Synthesis of carbon dots

The synthesis of carbon dots was carried out by first dissolving 1.0 g of OPD and 0.5 g of semicarbazide in DDW. The precursor solution was subsequently relocated to a Teflon-lined stainless-steel autoclave, where it underwent hydrothermal processing. The sealed autoclave was heated in an oven at 180 °C for 6.0 h. After the reaction time, the autoclave was left to cool down to room temperature. The produced suspension was subjected to centrifugation at 10,000 rpm for 10 min to remove any large particles or agglomerates. The supernatant was carefully collected and loaded into a dialysis bag with a molecular weight cut-off (MWCO) of 1,000 Daltons (Da). Dialysis was performed against DDW to get rid of any unreacted precursors. Finally, the purified carbon dot solution was subjected to freeze-drying, and the obtained carbon dot powder was stored at 4 °C for further use and characterization.

2.4. Fluorescence quantum yield measurement

The quantum yield steps and calculations of NRECDs are documented in the supplementary data file.

2.5. Preparation of Zn-dithizone complex

The following procedure for preparing the zinc-dithizone complex is based on previously reported methods [24–26]. 50 μL of a 1.0 mM dithizone solution in chloroform was added to 2.5 mL of a 0.1 M Tris-HCl buffer (pH 8.0) containing 0.5 % SDS, followed by the addition of 25 μL of a 10.0 mM zinc acetate solution; the mixture was vortexed vigorously for 2 min to promote the formation of the zinc-dithizone complex, which exhibited a distinct red color; the resultant solution was subjected to dilution to 5.0 mL with the Tris-HCl buffer containing 0.5 % SDS.

2.6. Detection of urea

For urea detection, 500 μL of prepared NRECDs, 1.0 mL of Zn-dithizone and 100 μL urease solution (1.0 mg mL^{-1}, dissolved in 10.0 mM phosphate buffer at pH 7.0) and were transferred into a 10.0 mL volumetric flask. Following this, 100 μL of various urea concentrations were added into the previous mixture. Then volume completed to the

mark using double distilled water. The prepared samples were incubated at a temperature of 37 °C for duration of 30 min. Post-incubation, fluorescence spectra were measured, using an excitation wavelength of 565 nm.

2.7. Analysis of urea in human serum

An assay system utilizing urease/NRECDs/Zn-dithizone was employed to measure urea concentrations in human serum samples collected from three healthy young male volunteers from three different regions in Assiut governate, Egypt. Initially, the blood samples were subjected to centrifugal force at 10,000 rpm for 20 min, facilitating the separation of the supernatant from the rest of the sample. Subsequently, 2.0 mL of acetonitrile was added to 0.5 mL of this supernatant, followed by vortex shaking for 5 min. This mixture was then centrifuged under the same conditions for an additional 20 min. The resulting supernatant was diluted tenfold with deionized water and the pH was adjusted to 7.0. To create spiked samples for analysis, varying amounts of urea were added to these diluted supernatants.

2.8. Analysis of urea in human urine

To evaluate the effectiveness of our urea detection method in urine samples, we analyzed urine samples from three healthy young male volunteers from three different regions in Assiut governate, Egypt. The samples were diluted 100-fold before analysis to bring the urea concentration within the detectable range. We adapted the urea determination protocol described in section 2.6, replacing the urea standard solution with the diluted urine sample. To validate the method's accuracy and investigate potential interference from other urinary components, we performed a recovery study. This involved spiking the diluted urine samples with known amounts of urea at three different concentrations (0.01, 0.3, 1.0 and 2.5 mM). We then analyzed these spiked samples using our modified procedure. The recovery rates were determined by comparing the measured urea concentrations in the spiked samples to the expected values, considering the baseline urea levels present in the unspiked urine samples. The experimental procedures summarizing determination of urea in human serum and human urine are shown in Scheme 1.

3. Results and discussion

3.1. Morphological and structural characterization

Transmission electron microscopy (TEM) characterization offers an in-depth look at the morphological characteristics and size range of NRECDs. Carbon dots are monodispersed and exhibit a near-spherical morphology, as evidenced by TEM characterization (Fig. 1A). The inset of TEM images typically shows a particle size distribution ranging from 2 to 6 nm, with an average particle size of around 3.5 nm.

The Fourier-transform infrared (FTIR) spectrum of NRECDs reveals several characteristic peaks that can be attributed to specific functional groups (Fig. 1B). The forked peak observed at 3134 and 3031 cm^{-1} assigned to the stretching oscillations of O–H and N–H bonds, verifying the presence of hydroxyl and amine groups on the carbon dot surface [15,27]. The shoulder peak at 2801 cm^{-1} is related to the stretching vibrations of C–H bonds, suggesting the presence of alkyl groups. The sharp peak at 1737 cm^{-1} is attributed to the stretching vibrations of C = O bonds, indicating the existence of carbonyl groups [16,28]. The small peak at 1626 cm^{-1} can be attributed to the stretching oscillations of C = C bonds, indicative of aromatic or alkene structures. The peak at 1486 cm^{-1} is characteristic of the bending vibrations of C–H bonds. Additionally, the peaks observed at 1260, 1200, 1095, 962, 741, 599, and 510 cm^{-1} can be ascribed to various stretching and bending vibrations of C-O, C-N, and C–C bonds, suggesting the presence of ether, amine, and alkyl groups on the carbon dot surface [29,30].

The X-ray diffraction (XRD) characterization of carbon dots often reveals a broad peak centered around 21.2 degrees (2θ). This broad diffraction peak is indicative of the amorphous nature of these nanomaterials, suggesting a lack of long-range crystalline order within their

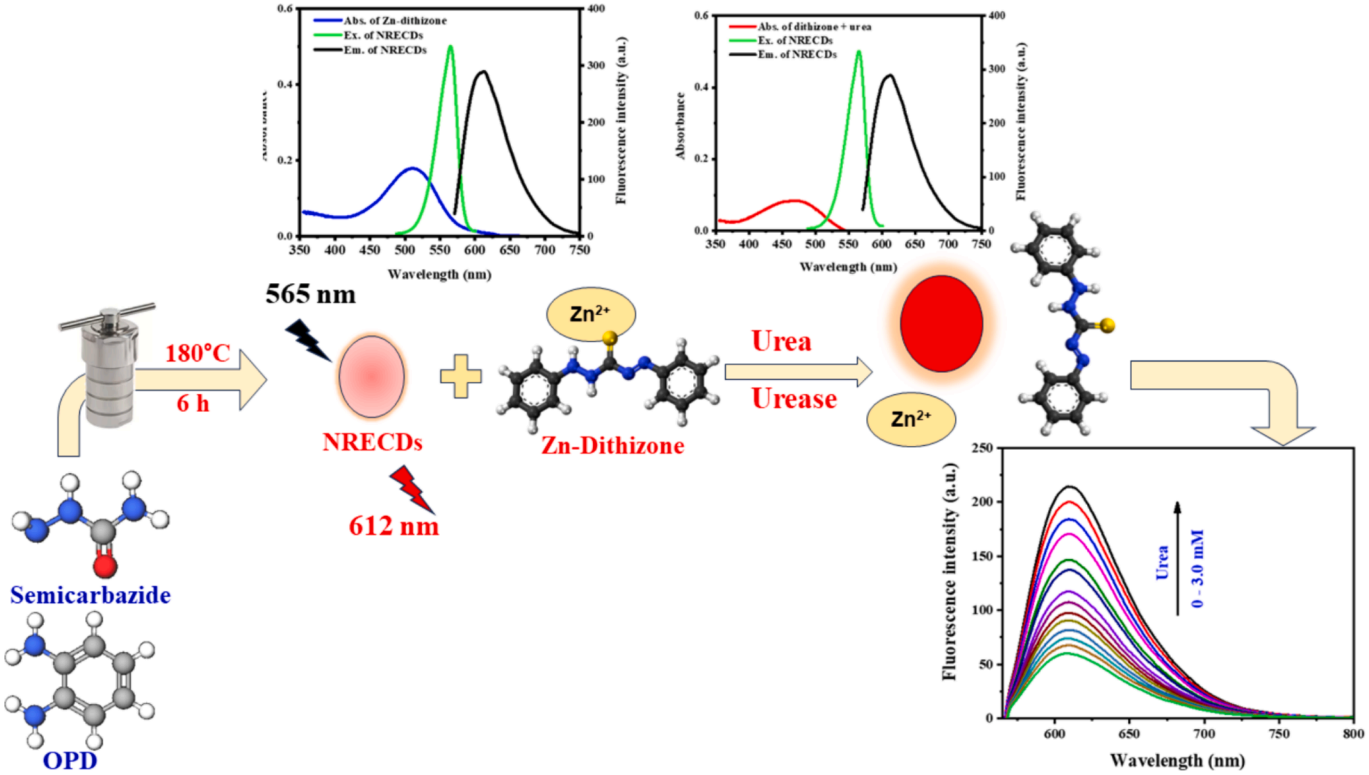

Scheme 1. Schematic presentation representing determination of urea.

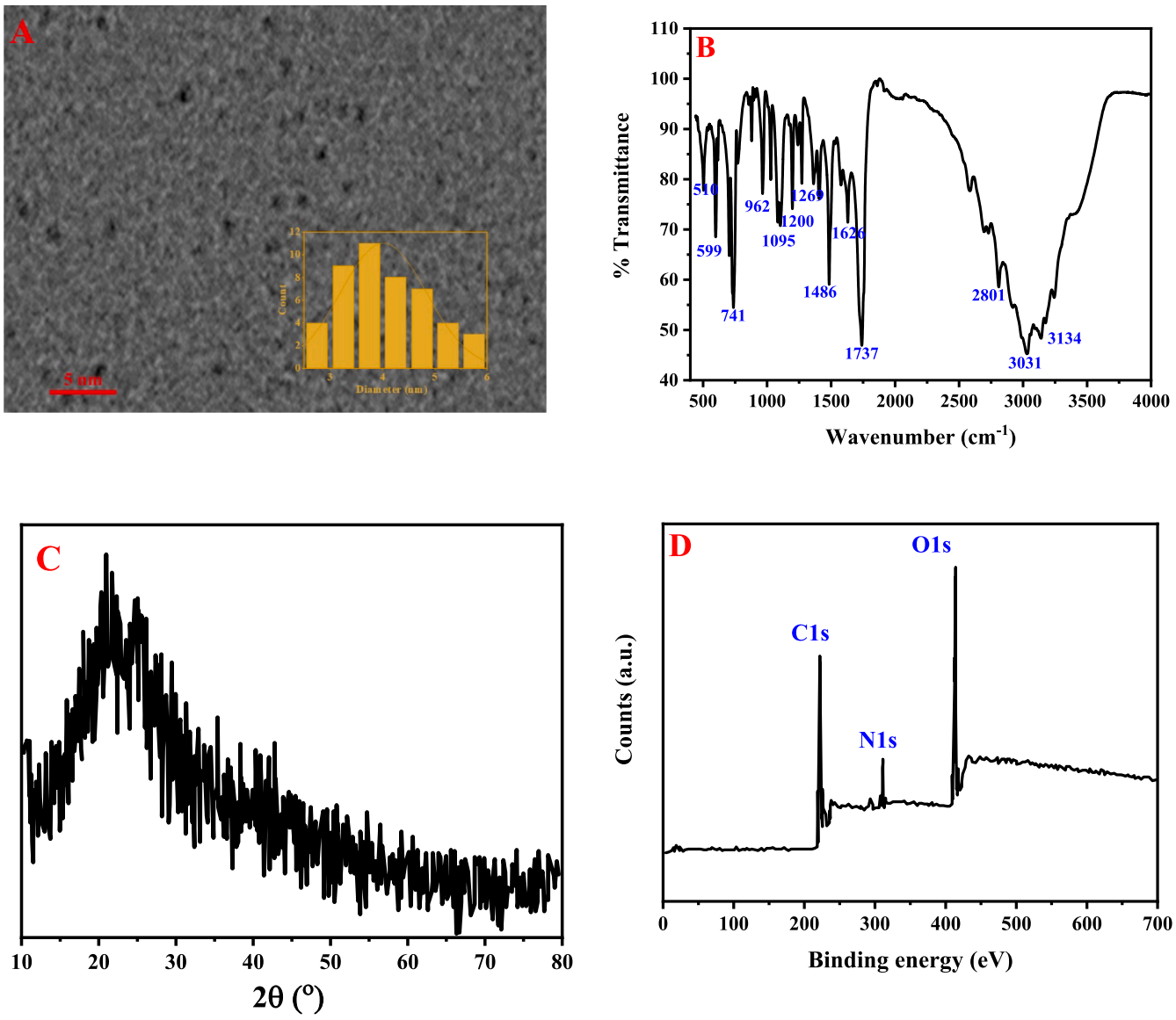

Fig. 1. (A) The TEM image (Inset: The size distribution of NRECDs particles), (B) The FT-IR spectrum, C) XRD patterns and D) XPS patterns of NRECDs nanoparticles.

structure (Fig. 1C). The elemental composition and presence of surface functional groups in the NRECDs were investigated through X-ray Photoelectron Spectroscopy (XPS) analysis. The comprehensive XPS spectra obtained for the NRECDs exhibited peaks at binding energies of 284.59 eV, 399.72 eV, and 529.47 eV, corresponding to the C1s, N1s, and O1s core levels, respectively (Fig. 1D). These peaks confirmed the existence of carbon, nitrogen, and oxygen elements within the NRECDs [31–33].

In the detailed C 1 s spectra (Fig. S1A), peaks were discerned at 288.32 eV, 285.47 eV, and 284.69 eV, corresponding to C = O, C-O/C-N, and C–C bonds, respectively. The N 1 s spectra (Fig. S1B) exhibited peaks at 400.21 eV, 399.52 eV, and 399.1 eV, representing amino N, pyrrolic N, and pyridinic N functionalities, respectively. Likewise, the O1s spectrum (Fig. S1C) showed two peaks at 530.92 eV and 529.43 eV, associated with C = O and C-O bonds, respectively [17,33,34].

3.2. Optical characterization

Various spectroscopic techniques are utilized to characterize the optical characteristics and electronic structure of NRECDs. The UV–Vis absorption spectrum reveals three the following peaks: a peak at 226 nm, ascribed to π-π* transitions of aromatic carbon cores; a sharp peak at 278 nm, arising from the n-π* transitions of C = O bonds; and a broad, small peak at 422 nm, indicative of the presence of conjugated system within the carbon dot structure (Fig. 2A). Photoluminescence spectroscopy is crucial for probing the emission characteristics of these nanomaterials. By changing the excitation wavelengths from 520 to 590 nm, the photoluminescence intensity and corresponding wavelengths can be recorded (Fig. 2B). Notably, the highest emission intensity is often observed upon excitation at 565 nm [31]. One of the remarkable features of carbon dots is their excitation-independent emission behavior. This phenomenon is characterized by the observation that the emission peak position, typically around 612 nm, remains unchanged despite varying the excitation wavelengths. This behavior is attributed to the presence of surface defects or emissive trap states within the carbon dot structure, which act as the dominant emission centers. These trap states are responsible for the observed emission, and their energy levels remain unaffected by the excitation wavelength, leading to the excitation-independent emission behavior [31].

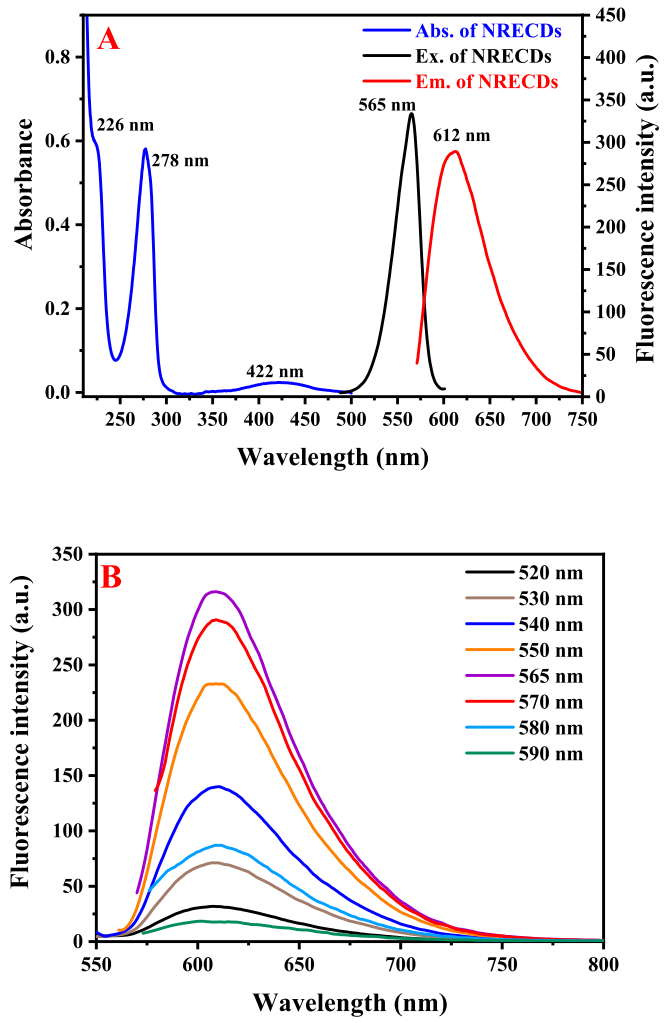

Fig. 2. (A) UV–Vis absorption, excitation, and emission spectra of NRECDs. (B) Fluorescence spectrum of NRECDs excited from 520 to 590 nm, at 10 nm intervals of wavelength.

3.3. Carbon dots stability

Carbon dots exhibit remarkable stability under a wide range of conditions, making them attractive for various applications. The effects of pH on their fluorescence intensity have been investigated, revealing that these nanomaterials maintain stable emission within the pH range from 5.0 to 11.0 (Fig. S2A). Furthermore, the ionic strength of the solution has been evaluated by varying the concentration from 0.01 M to 2.0 M. Remarkably, no notable change in the photoluminescence intensity of carbon dots was observed over this broad range of ionic strengths (Fig. S2B). This robustness against ionic interactions highlights their potential for use in complex media. The stability of carbon dots under UV irradiation has also been assessed by exposing them to UV light for durations ranging from 0.0 to 6.0 h (Fig. S2C). Impressively, no measurable change in their fluorescence intensity was detected, indicating their resistance to photodegradation. Additionally, the effects of temperature on the fluorescence intensity of carbon dots have been investigated within the range of 20 to 80 °C (Fig. S2D). While a slight decrease in emission intensity was noticed with increasing temperature, the overall stability of these nanomaterials across this temperature range is noteworthy, suggesting their potential for use in applications involving varying thermal conditions.

3.4. Optimization of reaction conditions

The interaction between zinc-dithizone complex and NRECDs presents an intriguing phenomenon that can be utilized for urea sensing. Dithizone forms a colored complex with zinc ions, and the color of this complex is highly dependent on the pH of the solution. Over the pH range of 4.0 to 12.0 (Fig. S3A), the color and formation of the zinc-dithizone complex exhibit distinct behaviors. At pH values in the range from 5.0 to 8.0, the zinc-dithizone complex forms a distinct red color. Interestingly, this red complex can quench the fluorescence of NRECDs. However, at higher pH values, upon the release of ammonia, the zinc-dithizone complex dissociates, and the free dithizone molecule adopts a yellow color. Remarkably, this dissociation leads to the restoration of the carbon dots' fluorescence. The restoration of fluorescence can be explained by the absence of the quenching effect due to the dissociation of the zinc-dithizone complex [24,35,36], allowing the carbon dots to emit their characteristic fluorescence. Furthermore, the volume of the added zinc-dithizone solution plays a crucial role in the quenching process. It has been observed that a volume of 1.0 mL is sufficient to cause substantial quenching of the carbon dots' fluorescence (Fig. S3B). This pH-dependent behavior of the zinc-dithizone complex and its ability to quench and restore the fluorescence of NRECDs presents exciting opportunities for developing sensitive and selective sensing platforms for the detection and quantification of ammonia released from urea degradation.

The amount of ammonia released upon the action of urease on urea is influenced by several factors, including urease concentration, reaction time, and reaction temperature. These factors are pivotal in optimizing the enzymatic hydrolysis of urea, ensuring efficient ammonia production and subsequent fluorescence restoration. Urease concentration is a key factor that determines the rate and extent of urea hydrolysis. In the studied range of 0.05–1.5 mg mL^{-1}, it was observed that a concentration of 1.0 mg mL^{-1} was sufficient to achieve complete hydrolysis of urea, even at the highest concentration within the calibration range (Fig. S3C). Enzymatic reaction time is critical in allowing the urease-catalyzed hydrolysis of urea to proceed to completion. By studying the reaction over a range of 0 – 60.0 min., it was determined that an optimum reaction time of 30.0 min. was required for efficient interaction between urea and urease (Fig. S3**D**). Longer reaction times did not result in further restoration of fluorescence, indicating that the reaction had reached equilibrium. Temperature is another important factor that influences the rate of the urease-catalyzed reaction. As the reaction temperature was raised from 10 °C to 40 °C, an increase in the reaction rate was observed, leading to the liberation of more ammonia and subsequent restoration of fluorescence. So. 37 °C was selected for further experiments, which aligns with previous studies [37]. This behavior can be attributed to the enhanced kinetics of the enzymatic reaction at higher temperatures, facilitated by increased molecular motion and favorable thermodynamic conditions. However, it is noteworthy that at temperatures above 50 °C, the fluorescence restoration began to decline (Fig. S3E). This phenomenon can be assigned to the potential denaturation or inactivation of the urease enzyme at excessively high temperatures, which could impair its catalytic activity and consequently reduce the rate of urea hydrolysis and ammonia production [37].

3.5. Fluorescence detection of urea

The fluorescence system (urease/NRECDs/Zn-dithizone) constructed based on the pH-sensitive interaction between zinc-dithizone and NRECDs was employed for urea detection. As the concentration of urea increased from 0 to 3.0 mM, the fluorescence intensity of the initially quenched NRECDs gradually restored, as illustrated in Fig. 3A. The dissociation of the zinc-dithizone complex, triggered by the ammonia released through the urease-mediated enzymatic hydrolysis of urea, is responsible for the observed restoration of fluorescence, as it allows the NRECDs to regain their fluorescent capabilities. Fig. 3B depicts the

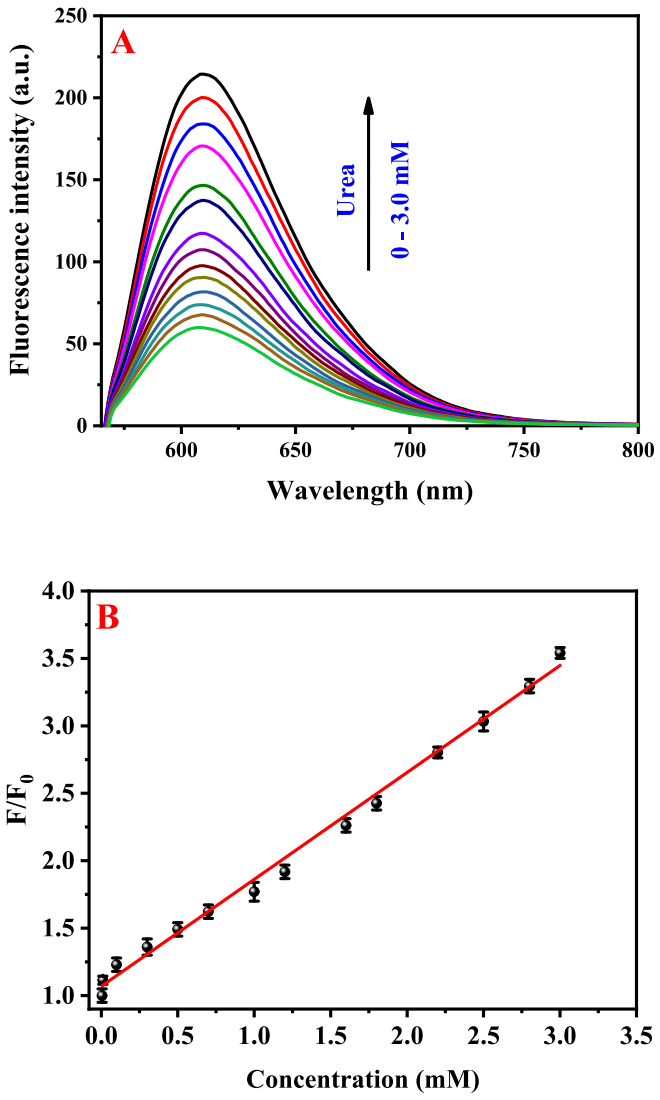

Fig. 3. (A) Fluorescence spectra of the urease/NRECDs/Zn-dithizone system at different urea concentrations (0.0–3.0 mM). (B) Linear plots of the increased fluorescence intensity ratio (F/F_0) of the urease/NRECDs/Zn-dithizone system as a function of urea concentration. F_0 and F are emission intensities of the urease/NRECDs/Zn-dithizone system in the absence and presence of urea, respectively.

relationship between the photoluminescence intensity of NRECDs and urea concentration in the range of 0.0 to 3.0 mM. The regression equation was determined to be $F/F_0 = 0.79\ [C_{urea}] + 1.07$, with a correlation coefficient (R^2) of 0.9951, indicating a strong linear relationship between (F/F_0) and urea concentration. Based on a signal-to-noise ratio (S/N) of 3, the detection limit for urea was calculated to be 0.0012 mM, demonstrating the sensitivity of this fluorescence-based system for urea detection. Furthermore, a comparison with previously reported methods for urea sensing was shown in **Table S1**.

The proposed method offers several notable advantages over previous methods. In terms of selectivity, this approach addresses limitations seen in some earlier methods. For instance, some methods relied solely on pH-sensitive carbon dots or quantum dots [20,37,38], which could be affected by other factors influencing pH in complex samples. The proposed method's use of the zinc-dithizone complex as a selective quencher that dissociates in the presence of urea-generated ammonia provides an additional layer of specificity. Regarding sensitivity, the proposed method demonstrates excellent performance with a limit of detection of 0.0012 mM. This is superior to all previous methods. Cost-effectiveness is another advantage of the proposed method. The use of carbon dots synthesized from relatively inexpensive precursors (OPD and semicarbazide) through a simple hydrothermal process is more economical compared to methods using other quantum dots [23,39,40]. This aspect is particularly important for potential large-scale or routine applications. In terms of ease of use, the proposed method offers a straightforward approach that doesn't require the multi-step procedures required for QDs functionalization or sol–gel membrane preparation [23,41,42]. The "mix-and-measure" nature of the assay makes it user-friendly and potentially more reproducible. Thus, the proposed method combines high selectivity, sensitivity, cost-effectiveness, and simplicity, making it a superior choice for practical urea detection applications.

To verify the precision of the (urease/NRECDs/Zn-dithizone) sensor, we examined the variability in fluorescence responses across different batches and among parallel samples within the same batch under optimal detection conditions. As shown in **Fig. S4**, the sensor demonstrated maximum relative standard deviations (RSD) of 2.21 % for urea detection across six different batches and 2.02 % for three parallel samples within the same batch. These results indicate that the developed (urease/NRECDs/Zn-dithizone) fluorescence sensor has high precision.

3.6. Selectivity and interference studies

The selectivity of a fluorescence system is a crucial parameter that determines its practical applicability. To assess the selectivity of the proposed fluorescence-based urea detection method, the effects of various potentially interfering substances were evaluated. These substances included inorganic salt ions (K^+, Zn^{2+}, Ca^{2+}, Mg^{2+}, Cu^{2+}, Fe^{3+}) and biomolecules commonly found in biological samples (Alanine (Ala), glycine (Gly), threonine (Thr), arginine (Arg), histidine (His), lysine (Lys), phenylalanine (Phe), fructose (Fru), glucose (Glu) and human serum protein (HSP) (**Fig. S5**). The investigation revealed that in the absence of urea, the presence of these coexisting substances had no significant effect on the fluorescence response of the system when compared to the blank sample. Furthermore, when urea was introduced in the presence of these coexisting substances, the relative errors in the urea detection were found to be less than 5 %. This minimal interference effect demonstrates the robustness of the proposed method, as the coexisting substances did not substantially influence the accurate determination of urea concentrations. These findings collectively highlight the exceptional selectivity of the proposed method for urea detection. The negligible responses to various inorganic salts and biomolecules, coupled with the minimal interference in the presence of urea, underscore the method's ability to provide reliable and accurate urea measurements in complex sample matrices.

The remarkable selectivity of NRECDs towards urea detection can be ascribed to two key factors. Firstly, the quenching of NRECDs' fluorescence is triggered by the increase in pH and the subsequent color change of the zinc-dithizone complex from red to yellow. Notably, the potentially interfering substances present at low concentrations found in diluted serum samples exert minimal influence on the pH of the phosphate buffer (pH = 7.0). Consequently, these substances do not induce the corresponding quenching effect, thereby ensuring the specificity of the system towards urea detection. Secondly, the long-wavelength excitation employed (565 nm) effectively minimizes the interference from endogenous autofluorescence backgrounds commonly present in complex biological matrices such as serum samples. This strategic choice of excitation wavelength allows for the selective excitation of the NRECDs while suppressing the contribution of autofluorescence, further enhancing the specificity and accuracy of the developed method.

3.7. Detection mechanism

The sensing mechanism of the proposed detection system (urease/NRECDs/zinc-dithizone) is based on the pH change induced by the

release of ammonia upon the enzymatic action of urease on urea. This pH-responsive system undergoes a remarkable transformation, enabling the sensitive detection of urea. Initially, the detection system is in a quenched state due to the presence of the zinc-dithizone complex, which exhibits a distinct red color with an absorption maximum around 511 nm. This red color of the zinc-dithizone complex leads to a spectral overlap with the excitation spectrum of the NRECDs, resulting in efficient fluorescence quenching through possible inner filtration effect. With the addition of urea, the urease enzyme initiates the hydrolysis reaction, causing the breakdown of urea and the subsequent liberation of ammonia. The released ammonia causes an increase in the pH of the solution, triggering a significant change in the zinc-dithizone complex. At higher pH values, the zinc-dithizone complex dissociates, and the free dithizone molecule adopts a yellow color with an absorption maximum around 460 nm (Fig. 4A). Crucially, this color change from red to yellow effectively eliminates the spectral overlap between the dithizone and the excitation spectrum of the NRECDs. Consequently, the efficient inner filter effect responsible for quenching is disrupted, leading to the restoration of the NRECDs' fluorescence (Fig. 4B). The sensing mechanism relies on this pH-induced dissociation of the zinc-dithizone complex and the subsequent spectral shift, which modulates the fluorescence intensity of the NRECDs. By monitoring the changes in emission intensity, the concentration of urea can be quantified with high sensitivity and selectivity. This unique sensing strategy exploits the pH-responsive behavior of the zinc-dithizone complex, coupled with the fluorescence properties of NRECDs, to create a versatile and effective detection system for urea.

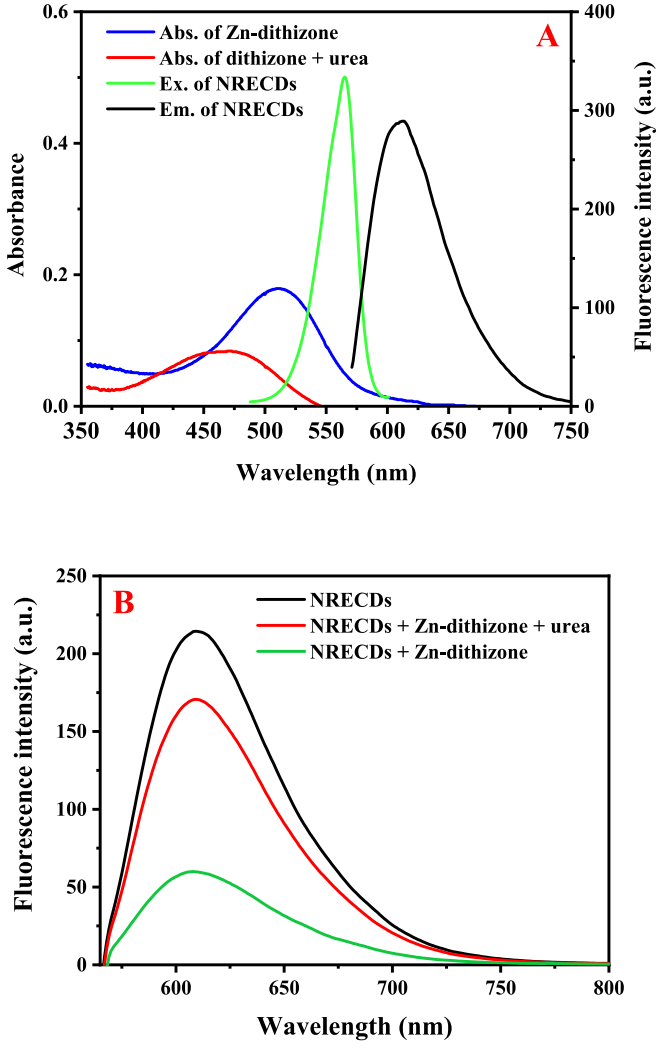

Fig. 4. (A) Spectral overlay of UV–Vis absorption of zinc-dithizone, UV–Vis absorption of zinc-dithizone + 1.0 μM urea, excitation spectra of NRECDs, and emission spectra of NRECDs. **(B)** Spectral overlay of fluorescence of NRECDs, NRECDs/ zinc-dithizone, and NRECDs/ zinc-dithizone /urea.

To provide further insights into the proposed sensing mechanism, fluorescence lifetime measurements were conducted (Fig. S6). The results revealed slight changes in the photoluminescence lifetimes of the NRECDs before and after the addition of zinc-dithizone complex, with values of 4.86 ns and 4.62 ns, respectively. The observed quenching and subsequent fluorescence restoration can be attributed to the inner filter effect (IFE), as evidenced by this observation, dismissing the possibility of Förster resonance energy transfer (FRET) mechanisms being the underlying cause. The absence of a significant change in the fluorescence lifetime suggests that FRET is unlikely to be the dominant mechanism. However, the minimal variation in the fluorescence lifetimes suggests that the quenching and restoration processes are not driven by FRET but IFE.

To test the reversibility of the system involving urease, NRECDs, and the zinc-dithizone complex in response to pH changes due to varying urea concentrations, a series of cyclic experiments were performed. The concentration of urea was adjusted from 0.5 to 3.0 mM and then reduced back to 0.5 mM over six cycles. The results, as displayed in Fig. S7, showed the photoluminescence of the system remained consistent, with only a 1.8 % variation in intensity. This consistency confirms the system's stability and validates the pH-induced reversible dissociation mechanism of the zinc-dithizone complex under fluctuating urea concentrations and pH levels.

3.8. *Determination of urea in human serum and urine samples*

In order to explore the practical applications of this method, the detection of urea in human serum and human urine was conducted. Known amounts of standard urea samples were intentionally added to the samples, and their respective recovery values were calculated to validate the accuracy of the sample analysis procedure. The results obtained for the urea concentration measurements in human serum and urine samples fell within the expected range of standard values for urea levels in human urine and serum (Table 1 **and** Table 2). Notably, the average recoveries of urea in the real samples ranged from 96.80 % to 102.00 %, with a low RSD of less than 3.28 %. These findings demonstrate the feasibility and reliability of the developed method. To validate our proposed urea detection method, we conducted a comparative analysis with an established electrochemical technique [43], as described in the literature. The comparison revealed comparable recovery results between the two methods, with no statistically significant differences observed. This concordance between our approach and the established electrochemical method serves to reinforce the reliability and accuracy of our system for quantifying urea in complex biological matrices such as urine and serum samples.

4. Conclusion

This study successfully developed a novel fluorometric method for urea determination using nitrogen-doped red-emissive carbon dots (NRECDs), zinc-dithizone complex, and urease. The method demonstrates high sensitivity, excellent linearity, and superior selectivity compared to previous pH-sensitive carbon dot-based approaches. The unique combination of NRECDs and zinc-dithizone complex enables specific detection of urea through enzymatic hydrolysis, overcoming the limitations of non-specific pH responses. With a low detection limit and minimal interference from potentially interfering substances, this method shows great promise for accurate urea quantification. Its excellent performance in human serum samples, evidenced by high recovery rates and low relative standard deviations, underscores its potential for practical applications in biomedical and clinical settings. This innovative approach represents a significant advancement in urea

Table 1
Results of the analysis of urea in human serum samples ($n = 3$).

Samples	Proposed method				Reported method		
	Added (mM)	Found (mM)	Recovery %	RSD %	Found (mM)	Recovery %	RSD %
Sample 1	0	0.090	–	–	0.095	–	–
	0.1	0.192	102.00	2.50	0.193	98.00	2.23
	0.3	0.389	99.67	2.42	0.388	97.67	2.91
	1.0	1.072	98.20	1.58	1.066	97.10	1.95
	2.5	2.55	98.40	1.85	2.578	99.32	1.99
Sample 2	0	0.082	–	–	0.078	–	–
	0.1	0.179	97.00	3.12	0.177	99.00	2.99
	0.3	0.374	97.33	2.99	0.37	97.33	2.33
	1.0	1.05	96.80	2.25	1.066	98.80	2.98
	2.5	2.505	96.92	1.98	2.562	99.36	1.65
Sample 3	0	0.079	–	–	0.088	–	–
	0.1	0.177	98.00	2.81	0.187	99.00	2.85
	0.3	0.375	98.67	2.31	0.381	97.67	1.65
	1.0	1.053	97.40	3.15	1.067	97.90	1.99
	2.5	2.598	100.76	1.06	2.552	98.56	2.87

Table 2
Results of the analysis of urea in human urine samples ($n = 3$).

Samples	Proposed method				Reported method		
	Added (mM)	Found (mM)	Recovery %	RSD %	Found (mM)	Recovery %	RSD %
Sample 1	0	0.0068	–	–	0.0070	–	–
	0.1	0.106	99.20	3.12	0.105	98.00	2.95
	0.3	0.312	101.73	3.28	0.309	100.67	2.41
	1.0	1.011	100.42	2.21	1.004	99.70	1.58
	2.5	2.551	101.77	2.85	2.461	98.16	1.11
Sample 2	0	0.0071	–	–	0.0083	–	–
	0.1	0.105	97.9	2.32	0.108	99.70	3.21
	0.3	0.302	98.3	2.85	0.308	99.90	1.85
	1.0	1.002	99.49	2.74	1.014	100.57	2.36
	2.5	2.501	99.76	2.01	2.465	98.27	1.58
Sample 3	0	0.0056	–	–	0.0066	–	–
	0.1	0.103	97.40	2.95	0.105	98.40	2.33
	0.3	0.303	99.13	1.82	0.302	98.47	2.85
	1.0	1.012	100.64	2.36	1.006	99.94	1.98
	2.5	2.511	100.22	1.93	2.455	97.94	1.74

sensing technology, offering a reliable and efficient tool for urea detection in various fields.

CRediT authorship contribution statement

Khalid Alhazzani: Visualization, Validation, Project administration, Funding acquisition, Formal analysis, Data curation, Conceptualization. **Ahmed Z. Alanazi:** Writing – original draft, Visualization, Software, Resources, Project administration, Funding acquisition, Formal analysis, Data curation. **Aya M. Mostafa:** Writing – review & editing, Writing – original draft, Visualization, Formal analysis, Data curation. **James Barker:** Writing – review & editing, Writing – original draft, Validation, Software, Resources, Conceptualization. **Hossieny Ibrahim:** Supervision, Resources, Project administration, Methodology, Funding acquisition, Formal analysis. **Mohamed M. El-Wekil:** Conceptualization, Funding acquisition, Investigation, Methodology, Project administration, Resources, Validation, Writing – review & editing. **Al-Montaser Bellah H. Ali:** Conceptualization, Funding acquisition, Investigation, Methodology, Project administration, Resources, Validation, Writing – review & editing.

Declaration of competing interest

The authors declare that they have no known competing financial interests or personal relationships that could have appeared to influence the work reported in this paper.

Data availability

Data will be made available on request.

Acknowledgments

The authors would like to extend their appreciation to the Researchers Supporting Project number (RSPD2024R593) at King Saud University, Riyadh, Saudi Arabia.

Appendix A. Supplementary data

Supplementary data to this article can be found online at https://doi.org/10.1016/j.microc.2024.111129.

References

[1] M. Alfadhel, F.A. Mutairi, N. Makhseed, F.A. Jasmi, K. Al-Thihli, E. Al-Jishi, M. AlSayed, Z.N. Al-Hassnan, F. Al-Murshedi, J. Häberle, T. Ben-Omran, Guidelines for acute management of hyperammonemia in the Middle East region, Ther. Clin. Risk. Manag. 12 (2016) 479–487.
[2] N. Emmanuel, N.V. Patil, S.R. Bhagwat, A. Lateef, K. Xu, H. Liu, Effects of different levels of urea supplementation on nutrient intake and growth performance in growing camels fed roughage based complete pellet diets, Anim. Nutr. 1 (2015) 356–361.
[3] R.S. Mathias, D. Kostiner, S. Packman, Hyperammonemia in urea cycle disorders: Role of the nephrologist, Am. J. Kidney Dis. 37 (2001) 1069–1080.
[4] S. Swify, R. Mažeika, J. Baltrusaitis, D. Drapanauskaitė, K. Barčauskaitė, Review: Modified Urea Fertilizers and Their Effects on Improving Nitrogen Use Efficiency (NUE), Sustainability 16 (2024) 188.

[5] J.K. Akada, M. Shirai, H. Takeuchi, M. Tsuda, T. Nakazawa, Identification of the urease operon in Helicobacter pylori and its control by mRNA decay in response to pH, Mol. Microbiol. 36 (2000) 1071–1084.
[6] I. Konieczna, P. Zarnowiec, M. Kwinkowski, B. Kolesinska, J. Fraczyk, Z. Kaminski, W. Kaca, Bacterial urease and its role in long-lasting human diseases, Curr. Protein Pept. Sci. 13 (2012) 789–806.
[7] S.B. Adeloju, S.J. Shaw, G.G. Wallace, Polypyrrole-based potentiometric biosensor for urea part 1. Incorporation of urease, Anal. Chim. Acta 281 (1993) 611–620.
[8] M. Mascini, G.G. Guilbault, Urease coupled ammonia electrode for urea determination in blood serum, Anal. Chem. 49 (1977) 795–798.
[9] F. Kuralay, H. Özyörük, A. Yıldız, Amperometric enzyme electrode for urea determination using immobilized urease in poly(vinylferrocenium) film, Sens. Actuators b: Chem. 114 (2006) 500–506.
[10] J. Kawase, H. Ueno, A. Nakae, K. Tsuji, High-performance liquid chromatography of urea and related compounds with post-column derivatization, J. Chromatogr. A 252 (1982) 209–216.
[11] X. Zhu, X. Zhou, Y. Jing, Y. Li, Electrochemical synthesis of urea on MBenes, Nat. Commun. 12 (2021) 4080.
[12] M.C.G. Pellá, A.R. Simão, P. Valderrama, A.F. Rubira, A conventional and chemometric analytical approach to solving urea determination with accuracy and precision, Anal. Methods 15 (2023) 2016–2029.
[13] M.S. Abdel-Latif, G.G. Guilbault, Fluorometric determination of urea by flow injection analysis, J. Biotechnol. 14 (1990) 53–61.
[14] S.-I. Suye, J.J. Miura, M. Ohue, A fluorometric determination of urea with urease, Anal. Lett. 32 (1999) 1543–1551.
[15] A.Z. Alanazi, K. Alhazzani, A.M. Mahmoud, A.-M.-B.-H. Ali, M.M. El-Wekil, Advanced fluorescence-based determination of carboplatin, a potent anticancer agent, with tripeptide-functionalized copper nanoclusters, Microchem. J. 199 (2024) 110000.
[16] A.Z. Alanazi, K. Alhazzani, A.M. Mostafa, J. Barker, M.M. El-Wekil, A.-M.-B.-H. Ali, Highly selective fluorometric detection of streptokinase via fibrinolytic release of photoluminescent carbon dots integrated into fibrin clot network, Microchem. J. 197 (2024) 109800.
[17] K. Alhazzani, A.Z. Alanazi, A.M. Mostafa, J. Barker, M.M. El-Wekil, H.A.A. M. Bellah, A selective dual quenching sensor (EY/BG@CDs) for simultaneous monitoring of gentamicin and ketorolac levels in plasma: a highly efficient platform that caters to the needs of therapeutic drug monitoring, RSC Adv. 13 (2023) 28940–28950.
[18] K. Alhazzani, A.Z. Alanazi, A.M. Mostafa, J. Barker, M.M. El-Wekil, A.B.H. Ali, A novel microextraction technique aided by air agitation using a natural hydrophobic deep eutectic solvent for the extraction of fluvastatin and empagliflozin from plasma samples: application to pharmacokinetic and drug-drug interaction study, RSC Adv. 13 (2023) 31201–31212.
[19] J. An, Y. Hu, D. Yang, Y. Han, J. Zhang, Y. Liu, pH-induced highly sensitive fluorescence detection of urea and urease based on carbon dots-based nanohybrids, Spectrochim. Acta a: Mol. Biomol. Spectrosc. 269 (2022) 120705.
[20] S. Pang, A pH sensitive fluorescent carbon dots for urea and urease detection, Fuller. Nanotub. Carbon Nanostructures 28 (2020) 752–760.
[21] E. Safitri, L.Y. Heng, M. Ahmad, T.L. Ling, Fluorescence bioanalytical method for urea determination based on water soluble ZnS quantum dots, Sens. Actuators b: Chem. 240 (2017) 763–769.
[22] T. Shao, P. Zhang, L. Tang, S. Zhuo, C. Zhu, Highly sensitive enzymatic determination of urea based on the pH-dependence of the fluorescence of graphene quantum dots, Mikrochim. Acta 182 (2015) 1431–1437.
[23] H.D. Duong, J.I. Rhee, Use of CdSe/ZnS luminescent quantum dots incorporated within sol–gel matrix for urea detection, Anal. Chim. Acta 626 (2008) 53–61.
[24] M.S. Abdel-Latif, Direct Determination of Zinc Using Dithizone in Micellar Solution, Anal. Lett. 27 (1994) 2341–2353.
[25] K. Jabbar Ali, M. Kadoomm, J. Ali, Determination of zinc (II) ion using dithizone by flow injection and sequential injection techniques, Int. J. Chem. Sci. 16 (2018) 236.
[26] M.H. Memon, P.J. Worsfold, Analytical applications of microemulsions, spectrophotometric determination of zinc using dithizone, Analyst 113 (1988) 769–771.
[27] B.A. Alyami, A.M. Mahmoud, A.O. Alqarni, A.-M.-B.-H. Ali, M.M. El-Wekil, Ratiometric fluorometric determination of sulfide using graphene quantum dots and self-assembled thiolate-capped gold nanoclusters triggered by aluminum, Mikrochim. Acta 190 (2023) 467.
[28] K. Alhazzani, A.Z. Alanazi, A.M. Mostafa, J. Barker, M.M. El-Wekil, A.B.H. Ali, Cobalt-modulated dual emission carbon dots for ratiometric fluorescent vancomycin detection, RSC Adv. 14 (2024) 5609–5616.
[29] K. Alhazzani, A.Z. Alanazi, A.M. Mostafa, J. Barker, M.M. El-Wekil, A.B.H. Ali, Selective fluorescence turn-on detection of combination cisplatin-etoposide chemotherapy based on N-CDs/GSH-CuNCs nanoprobe, RSC Adv. 14 (2024) 2380–2390.
[30] K. Alhazzani, A.Z. Alanazi, A.M. Mostafa, J. Barker, M.M. El-Wekil, A.-M.-B.-H. Ali, A dual emissive silver-riboflavin complex and nitrogen-doped carbon dot nanoprobe for ratiometric detection of glutathione, Microchem. J. 199 (2024) 109996.
[31] Y.S. Alqahtani, A.M. Mahmoud, M.M. El-Wekil, A.-M.-B.-H. Ali, Selective fluoride detection based on modulation of red emissive carbon dots fluorescence by zirconium-alizarin complex: application to Nile River water and human saliva samples, Microchem. J. 198 (2024) 110184.
[32] A.H. Rageh, F.A.M. Abdel-aal, S.A. Farrag, A.-M.-B.-H. Ali, A surfactant-based quasi-hydrophobic deep eutectic solvent for dispersive liquid-liquid microextraction of gliflozins from environmental water samples using UHPLC/fluorescence detection, Talanta 266 (2024) 124950.
[33] A.-M.-I. Mohamed, N.A. Mohamed, A.M.B.H. Ali, Simultaneous Determination of Three 5-HT3 Receptor Antagonists Accompanied by Stability Study Using Thin-Layer Chromatography-Densitometry, J. Planar Chromatogr. - Mod. TLC. 32 (2019) 285–294.
[34] A.M.I. Mohamed, N.A. Mohamed, A.M.B.H. Ali, Development and validation of RP-HPLC method for simultaneous determination of ondansetron hydrochloride and granisetron hydrochloride in their admixtures with pantoprazole sodium, Thai, J. Pharm. Sci. 44 (2020) 82–90.
[35] Q. Mei, W. Deng, W. Yisibashaer, H. Jing, G. Du, M. Wu, B.N. Li, Y. Zhang, Zinc-dithizone complex engineered upconverting nanosensors for the detection of hypochlorite in living cells, Small 11 (2015) 4568–4575.
[36] M.K. Song, N.F. Adham, H. Rinderknecht, A simple, highly sensitive colorimetric method for the determination of zinc in serum, Am. J. Clin. Pathol. 65 (1976) 229–233.
[37] F. Zhang, M. Wang, L. Zhang, X. Su, Ratiometric fluorescence system for pH sensing and urea detection based on MoS_2 quantum dots and 2, 3-diaminophenazine, Anal. Chim. Acta 1077 (2019) 200–207.
[38] W. Yin, Y. Zhang, J. Gu, T. Wang, C. Ma, C. Zhu, L. Li, Z. Yang, T. Zhu, G. Chen, Urea detection in milk by urease-assisted pH-sensitive carbondots, Appl. Opt. 60 (2021) 10421–10428.
[39] T. Oymak, N. Ertaş, U. Tamer, Use of water soluble and phosphorescent MPA-capped CdTe quantum dots for the detection of urea, Turk. J. Pharm. Sci. 15 (2018) 44–49.
[40] C.-P. Huang, Y.-K. Li, T.-M. Chen, A highly sensitive system for urea detection by using CdSe/ZnS core-shell quantum dots, Biosens. Bioelectron. 22 (2007) 1835–1838.
[41] S. Liu, F. Shi, L. Chen, X. Su, Dopamine functionalized CuInS2 quantum dots as a fluorescence probe for urea, Sens. Actuators B: Chem. 191 (2014) 246–251.
[42] H. Huang, J. Li, M. Liu, Z. Wang, B. Wang, M. Li, Y. Li, pH-controlled fluorescence changes in a novel semiconducting polymer dot/pyrogallic acid system and a multifunctional sensing strategy for urea, urease, and pesticides, Anal. Methods 9 (2017) 6669–6674.
[43] T.H.V. Kumar, A.K. Sundramoorthy, Non-enzymatic electrochemical detection of urea on silver nanoparticles anchored nitrogen-doped single-walled carbon nanotube modified electrode, J. Electrochem. Soc. 165 (2018) B3006.